Electrochemical recovery of Nd using liquid metals (Bi and Sn) in LiCl-KCl-$NdCl_3$

Sanghyeok Im, Nathan D. Smith, Stephanie Castro Baldivieso, Jarrod Gesualdi, Zi-Kui Liu, Hojong Kim*

Materials Science and Engineering, The Pennsylvania State University, 406 Steidle Building, University Park, PA 16802, United States

Author Email Addresses:

svi5106@psu.edu, nds174@psu.edu, szc6095@psu.edu, jqg5465@psu.edu, zxl15@psu.edu, huk29@psu.edu

Corresponding Author:

*E-mail: huk29@psu.edu. Tel: 814-865-3117. Fax: 814-865-2917

Keywords:

Electrochemical recovery, Rare-earth element, Neodymium, Liquid metal electrode, Nd alloys

Highlights

- Thermochemical properties of Nd in liquid Bi and Sn via reliable emf measurements
- Highly-efficient electrochemical recovery of Nd using liquid metal cathodes
- Facile charge-transfer kinetics (high exchange current) of Nd^{3+}/Nd in liquid metals
- High recovery capacity of liquid metals for Nd (20 mol%) beyond the solubility limit

ABSTRACT

Highly efficient recovery of Nd into liquid metals of Bi and Sn was achieved in molten LiCl-KCl-$NdCl_3$ electrolyte at 773–973 K by leveraging the strong interactions of Nd with liquid metals. Based on the emf measurements of Nd-Sn and Nd-Bi alloys, the activity values of Nd were determined as low as $1.1–5.8\times10^{-13}$ in both liquid metals at 973 K while the solubility of Nd was found to be 1.46 mol% in Sn and 5.65 mol% in Bi. Both liquid metals demonstrated high round-trip coulombic efficiencies (>99.3%) during deposition-removal cycles of 10–50 mA cm^{-2} and high recovery capacity up to approximately 20 mol% Nd beyond the solubility limit. In addition, a high Nd recovery yield (84–90%) with respect to the applied charge was confirmed based on chemical analysis of electrolysis products in Bi after constant current electrolysis (–50 mA cm^{-2}) at 873–973 K. Overpotentials during the Nd deposition process were attributed to charge-transfer and mass-transport resistances based on the current-potential curve and electrochemical impedance spectroscopy. The charge-transfer kinetics of Nd deposition into liquid metals was facile with high exchange current densities at ~220 mA cm^{-2}. The exceptionally high recovery efficiency for Nd in the molten chloride is thought to result from strong chemical interactions (i.e., low activity) of Nd in liquid metals that encourage one-step reduction, i.e., $Nd^{3+} + 3e \rightarrow$ Nd(in Bi or Sn) by effectively suppressing side reaction pathways from multivalent states (Nd^{2+} and Nd^{3+}).

1. INTRODUCTION

Electrochemical reduction processes using molten salts are widely employed in the primary production of rare-earth metals for clean energy technologies (e.g., NdFeB permanent magnets) and recycling used nuclear fuel (pyroprocessing) [1–3]. For example, Nd metal is produced by electrolysis at ~1100 °C in molten fluoride electrolyte (e.g., LiF-NdF_3) that can dissolve Nd_2O_3 up to ~2 wt%. The use of fluoride-based electrolytes have been favored over chloride-based electrolytes (e.g., KCl-$NdCl_3$) primarily due to higher current efficiency in molten fluorides (~80% at 1100 °C) compared to chlorides (<35–50% at 800 °C) despite higher cell operation temperatures [4–7]. Although the current efficiency varies depending on the external factors (e.g., electrolyte composition, operating temperature, current density), the low current efficiency in chloride system has been fundamentally attributed to the multivalent states of Nd (Nd^{3+} and Nd^{2+}) that can (1) consume the current without producing Nd metal by partial reduction ($Nd^{3+} + e \rightarrow Nd^{2+}$) during electrolysis and (2) result in the loss of deposited Nd metal by disproportionation reaction ($2Nd^{3+} + Nd^0 \rightarrow 3Nd^{2+}$) [8–10]. In contrast, the relatively high efficiency in molten fluorides is attributed to increased stability of higher valence state of rare-earth elements in the salt [4].

In electrorefining of used nuclear fuel in molten salt electrolyte (LiCl-KCl), rare-earth metal fission products in the used fuel anode oxidize and accumulate in the electrolyte as the standard potentials of rare-earth elements are more negative than those of actinide elements in the chloride system [2,3,11]. To minimize the volume of nuclear wastes generated by recycling processes for used nuclear fuel, the electrolyte may be reused by eliminating the dissolved fission products including rare-earth elements. The dissolved rare-earth elements can be recovered from molten salts by electrodeposition (lanthanide drawdown), following the recovery of actinides (actinide drawdown) [1–3,12]. However, the electrochemical recovery of rare-earth elements in the chloride

system has been reported to be inefficient, typically less than <35–50% efficiency, due to the aforementioned side reaction pathways from multivalent states of rare-earth elements [3,6,13].

The present work investigated liquid metal electrodes (Bi and Sn) to enhance recovery efficiency of rare-earth elements from a molten chloride salt (LiCl-KCl-$NdCl_3$) by leveraging strong chemical interactions between Nd and the liquid metal [13–19]. In previous works, alkaline-earth elements (e.g., Ba^{2+}) with the most negative redox potentials were found to be recovered into liquid metals (e.g., Bi) from LiCl-KCl-$BaCl_2$ due to strong chemical interactions of Ba-Bi compared to Li-Bi and K-Bi [20,21]. Recent emf measurements on the Nd-Bi system by the authors confirmed that the activity of Nd in liquid Bi is extremely low ($a_{Nd} = 1.1 \times 10^{-13}$ at 973 K), utilizing a two-phase Nd-Sn alloy ($x_{Nd} = 0.10$) as a reference electrode in the electrochemical cell [22].

In evaluating recovery efficiency of liquid metals, the present work newly established the thermochemical properties of Nd-Sn alloys via emf measurements and compared to the prior results by Kulagina and Bayanov who employed pure Nd as a reference electrode in LiCl-KCl-$NdCl_3$ at 773–973 K [23]. Based on the emf results of Nd-Sn and Nd-Bi alloys, each liquid metal electrode was subjected to constant-current electrolysis for Nd recovery in LiCl-KCl-$NdCl_3$ system at 973 K up to 22 mol% Nd beyond the solubility limit. The recovery efficiencies of liquid metals were estimated based on deposition-removal cycles of Nd (round-trip coulombic efficiency) and chemical analysis of electrolysis products in the liquid metal electrode (Faradaic efficiency). Lastly, the current-dependent overpotentials of liquid metal electrodes were characterized to estimate charge-transfer and mass-transport resistances during electrodeposition of Nd, in complement with electrochemical impedance spectroscopy (EIS).

2. EXPERIMENTAL METHODS

2.1 Electrochemical cell components and assembly

All assembly of the electrochemical cell and its components was conducted in an Ar-filled glovebox (O_2 < 0.5 ppm and H_2O < 1.0 ppm) due to the hygroscopic nature of the electrolyte and oxygen affinity of the electrode materials.

Electrolyte: Ternary LiCl-KCl-$NdCl_3$ electrolyte (eutectic LiCl-KCl + 2 mol% $NdCl_3$) was prepared by mixing appropriate amounts of LiCl (Ultra dry, 99.9%, Alfa Aesar), KCl (Ultra dry, 99.95%, Alfa Aesar), and $NdCl_3$ (anhydrous, 99.5%, Alfa Aesar) powders. The mixed powder was poured into a quartz crucible (Technical Glass Products) for pre-melting in a stainless-steel vacuum chamber. The chamber was loaded into a crucible furnace (Mellen, CC-12), evacuated to ~1 Pa, and heated under vacuum at 373 K for 12 h and at 543 K for 12 h to dry the salt mixture. The chamber was then purged with ultra-high purity Ar gas and heated to 923 K for 3 h under a slowly flowing (50 mL min^{-1}) Ar atmosphere. After cooling, the dry and homogeneous electrolyte was ground into fine powder using a mortar and pestle for use in the electrochemical cell.

Electrodes: The working electrode (WE) was fabricated by melting pure Bi (99.999%, Sigma-Aldrich) or Sn (99.9999%, Alfa Aesar) in a BN crucible (17 mm height, 12 mm OD, 8 mm ID, and 15 mm depth, Saint Gobain) using an induction heater installed inside the glovebox. The approximate weight of each metal was 1.96–2.44 g for Bi and 2.03–2.38 g for Sn with a nominal surface area of 0.50 cm^2. The reference electrode (RE), an Nd-Sn alloy at $x_{Nd} = 0.10$, was fabricated using a laboratory arc-melter (MAM-1, Edmund Bühler GmbH) under an inert Ar atmosphere from pure Nd (99.1%, Alfa Aesar) and Sn metals. The Nd-Sn alloy RE was re-melted in a boron nitride (BN) crucible (25 mm height, 12 mm OD, 8 mm ID, and 20 mm depth) using the induction heater. Two 1 mm diameter capillary holes were drilled 7 mm above the bottom of the BN crucible to

establish contact with the electrolyte. The counter electrode (CE), an Nd-Bi alloy at x_{Nd} = 0.03, was fabricated by adding Nd pieces into liquid Bi in a BN crucible (15 mm height, 25 mm OD, 22 mm ID, and 10 mm depth) using the induction heater. Tungsten wires (1 mm diameter, 99.95%, Thermo shield) were inserted into each electrode as electrical leads during inducting melting. The three-electrode electrochemical cell configuration is shown in **Fig. 1.**

Cell assembly: The electrodes were placed in an alumina crucible (250 mL, 100 mm height, 60 mm OD, 52 mm ID, Advalue Technology) and the LiCl-KCl-$NdCl_3$ powder was poured over the electrodes. The electrochemical cell assembly was loaded into a stainless-steel test chamber, and the W electrical leads were insulated from the test chamber using alumina tubes (6.35 mm OD, 1.57 mm ID, and 304.8 mm length, Advalue Technology) which were sealed at the top with epoxy. The test chamber was sealed with top flange using O-ring inside the glovebox, loaded into a crucible furnace, and evacuated to ~1 Pa. The electrochemical cell was vacuum-dried using the same procedure for preparing the electrolyte, and heated to 773 K under flowing Ar. The cell temperature was measured using a thermocouple (ASTM, Type-K) located in the electrolyte and data acquisition system (NI 9211, National Instruments).

[Fig. 1]

2.2 Electrochemical measurements

Emf measurements of binary Nd-Sn alloys are based on the following electrochemical cell:

$$\underline{\text{Nd-Sn}(x_{Nd} = 0.10)} \mid \text{LiCl-KCl-NdCl}_3 \mid \text{Nd-Sn} \qquad (1)$$

where the underlined Nd-Sn alloy (x_{Nd} = 0.10) is the reference electrode (RE) and the Nd-Sn alloy at a given composition is the working electrode (WE). From the Nernst equation, the cell potential (E_I) is:

$$E_{\mathrm{I}} = -\frac{RT}{3F}\ln\left(\frac{a_{\mathrm{Nd}}}{a^{*}_{\mathrm{Nd}}}\right) \quad (2)$$

where a_{Nd} the activity of Nd in Sn, a^{*}_{Nd} is the activity of Nd in Sn at x_{Nd} = 0.10 (RE), R is the universal gas constant, T is the absolute temperature, and F is the Faraday constant. The emf of Nd-Sn at x_{Nd} = 0.10 (E_{RE}) relative to pure Nd was previously established using a solid CaF_2-NdF_3 electrolyte at 700–1100 K to generate the following relationship [24,25]:

$$E_{\mathrm{RE}} = -\frac{RT}{3F}\ln(a^{*}_{\mathrm{Nd}}) = 0.590 + 1.52 \times 10^{-4}\,T \ \ [\mathrm{V}] \quad \text{vs. Nd(s).} \quad (3)$$

Using Eqs. (2–3), the emf of Nd-Sn (E_{eq}) relative to pure Nd at a given temperature is obtained as follows:

$$E_{\mathrm{eq}} = E_{\mathrm{I}} + E_{\mathrm{RE}} = -\frac{RT}{3F}\ln(a_{\mathrm{Nd}}) = -\frac{\Delta\bar{G}_{\mathrm{Nd}}}{3F} \text{ vs. Nd(s)} \quad (4)$$

where $\Delta\bar{G}_{\mathrm{Nd}}$ is the change in partial molar Gibbs energy (chemical potential) of Nd.

Electrochemical measurements were conducted using a potentiostat-galvanostat (Autolab PGSTAT302N) at 773–973 K. The equilibrium potentials of various Nd-Sn alloy compositions were determined by coulometric titrations where Nd is electrodeposited into the Sn WE using a constant current of 10 mA cm^{-2} for 2795 s in each titration step, followed by an open-circuit potential (OCP) measurement for 2 h to allow for homogenization of the Nd-Sn alloy. The electrodeposited mass of Nd (m_{Nd}) was obtained using Faraday's law:

$$m_{Nd} = M_{Nd}\left(\frac{It}{3F}\right) \quad (5)$$

where M_{Nd} is the molar mass of Nd and I is the constant current applied for a time (t), to estimate the Nd composition of the electrode.

Each liquid metal (Bi or Sn) was subjected to deposition-removal cycles at various constant current densities (j = 10–150 mA cm^{-2}) to characterize the current-overpotential relation and round-trip coulombic efficiencies. At selected Nd compositions, electrochemical impedance

spectroscopy (EIS) was employed by applying a 5 mV amplitude over a 10^{-2}–10^{6} Hz frequency range. The collected impedance spectra were fitted to a Randles equivalent circuit model of *LR(Q(RW))*, where *L* is an inductor, *R* is a resistor, *Q* is a constant phase element, and *W* is a Warburg diffusion element. Lastly, each liquid metal WE was deposited to a selected composition up to 22 mol% Nd using a constant current of 50 mA cm^{-2}.

2.3 Characterizations of the electrodes

After electrochemical measurements, the electrochemical cell was cooled to room temperature for post-mortem characterization. Each WE was carefully separated from electrochemical cell assembly and was cut vertically in half using a low-speed diamond saw. The first half of the WE was mounted in epoxy, polished up to 1600 grit using silicon carbide abrasive paper and isopropyl alcohol, and characterized using a scanning electron microscope (SEM, FEI Quanta 200) fitted with an energy dispersive spectrometer (EDS) for morphological and compositional analyses. The other half of the WE was separated from the BN crucible, immersed in ethylene glycol for 24 h to dissolve the salt layer [26], and rinsed with isopropyl alcohol. The electrode was then pulverized into a fine powder using a mortar and pestle for chemical analysis by inductively coupled plasma-atomic emission spectroscopy (ICP-AES, Thermo iCAP 7400). The concentration of chlorine was also analyzed using ion chromatography (IC, Dionex ICS2100) to evaluate the residual salt content in the electrode.

3. RESULTS and DISCUSSION

3.1 Thermochemical properties of Nd-Bi and Nd-Sn alloys

The thermochemical properties of Nd alloys provide essential information regarding the strength of interactions between constituent elements (e.g., activity) and thus are critical for the design of efficient recovery processes using liquid metals. Due to the limited thermochemical data for Nd-Sn alloys, this work determined the emf values of Nd-Sn alloys using an electrochemical cell that employs two-phase [L + $NdSn_3$] alloy as the RE (Nd-Sn at x_{Nd} = 0.10) and liquid Nd-Bi (x_{Nd} = 0.03) as the CE (**Fig. 1**). The authors demonstrated the reliability of this electrochemical cell based on emf measurements of Nd-Bi alloys [22,24].

Emf measurements of Nd-Sn alloys: The composition of Nd-Sn alloys was changed sequentially via coulometric titration of Nd into liquid Sn using a constant current (10 mA cm^{-2}) at 773−973 K and the OCP was recorded following each titration step (**Fig. 2**a). At 973 K, the steady-state OCP shifted in the negative direction with the increase of Nd content in liquid state and reached a constant value at about 0.00 V vs. RE (Nd-Sn at x_{Nd} = 0.10) regardless of further increase in Nd content in the two-phase region. During the titration near the solubility limit, a steep potential drop was observed due to the formation of $NdSn_3$ intermetallic compounds (nucleation overpotential). Similar trends were observed at lower temperatures; however, the OCP (vs. RE) approached zero at an earlier titration step due to a lower solubility of Nd in liquid Sn.

[Fig. 2]

The emf value (E_I) at each composition was obtained from the average OCP for the last 0.5 h (dE/dt < 0.1 mV/h) and then converted to the emf (E_{eq}) versus pure Nd using the previously calibrated emf (E_{RE}) of the RE (Nd-Sn at x_{Nd} = 0.10) in Eq. 3 [24,25]. The emf of Nd-Sn alloy is plotted as a function of Nd composition using Faraday's law (Eq. 5) assuming a perfect coulombic efficiency for coulometric titration of Nd (**Fig. 3**). These emf values were used to calculate the activity (a_{Nd}) and excess partial molar Gibbs energy ($\Delta\bar{G}_{Nd}^{E}$), summarized in **Table 1**.

[Fig. 3] & [Table 1]

At 973 K, the emf decreases monotonically in the liquid phase with an increase in Nd concentration and remains constant in the two-phase L + $NdSn_3$ region where the activity of Nd is invariant with respect to the compositional change in the binary system due to the Gibbs phase rule. The distinct emf trajectories for the liquid single-phase and the L + $NdSn_3$ two-phase regions allow for the determination of the Nd solubility in liquid Sn from their intersection: 1.46 mol% Nd at 973 K (**Fig. 3**). At 773-873 K, there are insufficient emf data in the liquid phase and thus, the solubility was estimated from the onset of nucleation overpotential during titration (**Fig. 2**b), and the results are summarized in **Table 2**. It is noted that the estimated solubility (1.46 mol% Nd) from the onset of nucleation potential at 973 K (**Fig. 2**b), agrees with the value (1.46 mol% Nd) from the intersection of emf trajectories (**Fig. 3**). A high solubility of Nd in liquid Sn, e.g., 4.50 mol% at 973 K, by Eremenko et al. is believed to originate from insensitivity of differential thermal analyses (DTA) for detecting liquidus transitions for dilute Nd compositions [27].

[Table 2]

Compared to the emf of Nd-Sn alloys in this work at 773-973 K, the emf values from Kulagina and Bayanov [23] are different up to 46 mV for two-phase L + $NdSn_3$ region and do not exhibit clear phase transition between L and two-phase L + S regions (**Fig. 3**), leading to an overestimation of the Nd solubility (**Table 2**). This discrepancy is believed to come from the use of highly reactive Nd as the reference electrode in molten LiCl-KCl-$NdCl_3$, resulting in a disproportionation side reactions during their emf measurements [23].

At 973 K, both Nd-Sn and Nd-Bi alloys exhibited similarly high emf values (0.74–0.83 V vs. Nd) with extremely low activity (a_{Nd} = 1.1–5.8×10^{-13}), indicating strong chemical interaction

of Nd with these liquid metals (**Fig. 4**). In contrast, liquid Bi exhibited higher solubility for Nd (5.65 mol%) than Sn (1.46 mol%), suggesting a larger recovery capacity of Bi in liquid state.

[Fig. 4]

The round-trip coulombic efficiency of Bi and Sn electrodes was estimated at 973 K using a constant current of 10–50 mA cm^{-2} and a representative cycle at 50 mA cm^{-2} is presented in **Fig. 5**. High coulombic efficiencies were achieved of 99.51–99.96 % for Bi (estimated depth 4.1 mm at 973 K) and 99.31–100.40 % for Sn (estimated depth 6.9 mm at 973 K), suggesting the chemical reversibility of the electrode reaction and validating the data collected via the coulometric titration technique, thereby confirming its reliability for emf measurements of Nd-Sn and Nd-Bi.

[Fig. 5]

3.2 Electrochemical recovery of Nd into the liquid metals

To confirm highly efficient electrochemical recovery of Nd into strongly-interacting liquid metals, Bi and Sn cathodes were subjected to various constant current densities (10−150 mA cm^{-2}) in LiCl-KCl-$NdCl_3$ at 973 K, followed by post-mortem characterization of each electrode to estimate Faradaic efficiency based on chemical analysis of electrolysis products.

Liquid Bi: The overpotential of liquid Bi away from emf (E_{eq}) increases as the current increases from 10 to 150 mA cm^{-2} (**Fig. 6**a). Using a constant current at 50 mA cm^{-2}, Nd was electrodeposited into Bi electrodes near the solubility (6.50 mol% Nd) and beyond the solubility limit (22.2 mol%) for post-mortem characterization. For the Bi electrode at 6.50 mol% Nd (**Fig. 6**b), the NdBi intermetallic compound was observed near the electrode surface due to its lower density (8.86 g cm^{-3}) compared to Bi (9.78 g cm^{-3}) while the $NdBi_2$ compound was observed in the Bi matrix from solidification [28,29]. For the Bi electrode at 22.2 mol% Nd (**Fig. 6**c), the electrode was split into two parts, possibly due to an extensive formation of a solid phase (NdBi)

near the electrode surface. In this Bi electrode, the NdBi compound was mostly found at the electrode surface (II in **Fig. 6**c), and intermetallic compounds of Nd_3Bi_7 and $NdBi_2$ (I, III in **Fig. 6**c) were observed in the Bi matrix from solidification. The unstable potential behavior of the Bi electrode beyond the solubility limit is thought to originate from the formation/separation of solid intermetallic compounds with complex electrode morphology/growth behavior.

[Fig. 6]

The composition of the selected Bi electrode was analyzed by ICP-AES, and Faradaic recovery efficiency was estimated by taking into account the concentration of chlorine as the residual salt content from ion chromatography, summarized in **Table 3**. The Faradaic efficiency for Nd recovery was estimated to be 84–90% based on electrolysis products at 873–973 K, confirming a high recovery yield of Nd using liquid Bi in molten LiCl-KCl-$NdCl_3$. It is noted that Nd could be recovered far beyond the solubility limit while maintaining a high Faradaic efficiency, extending the capacity of liquid Bi for Nd recovery. The primary cause of Faradaic efficiency loss is thought to originate from the selective loss of Nd during sampling preparation for chemical analysis.

[Table 3]

Sn electrodes: The overpotential of the liquid Sn increases as current increases over 10−150 mA cm^{-2} at 973 K (**Fig. 7**a). Compared to liquid Bi, liquid Sn exhibited a sheer potential drop near the solubility limit (1.46 mol% Nd or 36 C g^{-1}) due to the nucleation of $NdSn_3$ compound. Using a constant current at 50 mA cm^{-2}, Nd was electrodeposited into Sn electrodes at 1.38 mol% near the solubility and 20.7 mol% beyond the solubility limit for post-mortem characterization. In the Sn electrode at 1.38 mol% Nd (**Fig. 7**b), the $NdSn_3$ intermetallic compound was mostly found near the bottom of the electrode possibly due to its higher density (7.97 g cm^{-3}) than liquid Sn (6.58 g

cm^{-3}) [29,30]. The segregation of $NdSn_3$ phase near the bottom of liquid Sn electrode was also observed by Kuriyama et al. during the electrochemical formation of Nd-Sn alloy at 723 K [31]. For the Sn electrode at 20.7 mol% Nd (**Fig. 7**c), the electrode was split into two parts after extensive formation of $NdSn_3$ compound, and the electrode potential was unstable during electrolysis beyond the solubility, similar to that found in the liquid Bi (**Fig. 6**c). The chemical analysis for Nd-Sn electrode was not successful due to the difficulty in dissolving the alloy in aqueous media for ICP-AES.

[Fig. 7]

3.3 Overpotential mechanisms in liquid metals

The current-dependent overpotentials of liquid Bi and Sn during Nd deposition (**Fig. 6**a and **Fig. 7**a) were analyzed to estimate the total resistance (R_{total}) during electrolysis at 973 K by constructing *I-V* curve at selected compositions (**Fig. 8**). For both Bi and Sn, a linear *I-V* relation was observed at 10–100 mA cm^{-2} but a deviation was observed at the highest current (150 mA cm^{-2}) for high Nd compositions. The area-specific resistance ($A \cdot R_{total}$) was estimated from the slope of linear fit (dE/dj), summarized in **Table 4**. The $A \cdot R_{total}$ tends to increase as Nd composition increases with the highest value near the solubility, e.g., from 0.41 Ω cm^2 to 0.71 Ω cm^2 for liquid Bi.

[Fig. 8] & [Table 4]

For detailed analysis of overpotential mechanisms, electrochemical impedance spectroscopy (EIS) was employed for each electrode at selected compositions, fitted to the Randles equivalent circuit model (**Fig. 9**), and results are summarized in **Table 4**. According to the EIS analyses, the charge transfer resistances (R_{ct}, semi-circle width) were nearly constant independent of Nd compositions for both electrodes (0.25−0.26 Ω cm^2), and the uncompensated ohmic resistances

(R_{ohm}, semi-circle intercept at high frequency) remained constant for each electrochemical cell, typical for three-electrode configurations. From the estimated R_{ct}, the exchange current density (j_0) was estimated at ~220 mA cm^{-2} using the following relation [32]:

$$j_0 = RT / 3F(A \cdot R_{ct}) \quad (6)$$

[Fig. 9]

To a first approximation, the R_{total} can be expressed as:

$$R_{total} = R_{ohm} + R_{ct} + R_{mt} \quad (7)$$

where R_{mt} is the mass transport resistance that can be estimated using the results from *I-V* curve (R_{total}) and EIS (R_{ohm} and R_{ct}). Using this relation, the relative contribution of each resistance in R_{total} was estimated at selected compositions (**Fig. 10**). This analysis suggests that the electrode process for Nd deposition into liquid Bi and Sn exhibits facile charge transfer kinetics with a high exchange current (~220 mA cm^{-2}) and the R_{mt} increases as Nd composition approaches the solubility limit, e.g., from 0.007 Ω·cm^2 to 0.298 Ω·cm^2 for liquid Bi.

[Fig. 10]

4. CONCLUSION

The emf measurements of Nd-Sn alloys at 773–973 K were conducted to quantify the strength of chemical interactions between Nd and Sn using a two-phase Nd-Sn alloy (x_{Nd} = 0.10) as the reference electrode. Both liquid Bi and Sn metals exhibited similarly high emf values which translate to extremely low activity of Nd (1.1–5.8×10^{-13}), confirming their strong chemical interactions with Nd. In addition, the solubility of Nd at 973 K was estimated at 1.46 mol% for liquid Sn, compared to 5.65 mol% for liquid Bi.

Utilizing the strongly interacting liquid metals, a high round-trip coulombic efficiency (>99.3%) was observed for liquid Bi and Sn in LiCl-KCl-$NdCl_3$ by effectively suppressing the

side reactions from the multivalent state of Nd ions in molten chloride solution at 973 K. Furthermore, this work successfully demonstrated that Nd can be recovered into liquid Bi up to 20.0 mol% beyond the solubility limit with a high Faraday efficiency (84–90%) based on the chemical analysis of electrolysis products by ICP-AES.

The electrode processes for Nd deposition into liquid Bi and Sn exhibit a facile charge transfer kinetics with exchange current density of ~220 mA cm^{-2} from EIS measurements at 973 K. The overpotentials tend to increase at high current densities (>150 mA cm^{-2}) and high Nd compositions due to increased mass transport resistances.

5. ACKNOWLEDGEMENTS

This work was supported by the U.S. Department of Energy (DOE) with Award No. DE-NE0008757 and the U.S. National Science Foundation (NSF) with Grant No. CBET-1844170.

REFERENCES

[1] M.F. Chambers, J.E. Murphy, Electrolytic Production of Neodymium Metal From a Molten Chloride Electrolyte, Pittsburgh, PA (United States), 1991.

[2] M.A. Williamson, J.L. Willit, PYROPROCESSING FLOWSHEETS FOR RECYCLING USED NUCLEAR FUEL, Nucl. Eng. Technol. 43 (2011) 329–334. https://doi.org/http://dx.doi.org/10.5516/NET.2011.43.4.329.

[3] M.F. Simpson, Developments of Spent Nuclear Fuel Pyroprocessing Technology at Idaho National Laboratory, United States, 2012. http://www.inl.gov/technicalpublications/Documents/5411188.pdf LK - https://www.osti.gov/servlets/purl/1044209/.

[4] H. Zhu, Rare Earth Metal Production by Molten Salt Electrolysis, in: G. Kreysa, K. Ota, R.F. Savinell (Eds.), Encycl. Appl. Electrochem., Springer New York, New York, NY, 2014: pp. 1765–1772. https://doi.org/10.1007/978-1-4419-6996-5_455.

[5] R.A. Sharma, Neodymium Production Processes, J. Met. 39 (1987) 33–37. https://doi.org/10.1007/BF03259468.

[6] C.K. Gupta, N. Krishnamurthy, Extractive Metallurgy of Rare Earths, 2005.

[7] R. Akolkar, Perspective — Is Sustainable Electrowinning of Neodymium Metal Achievable?, J. Electrochem. Soc. 169 (2022) 43501. https://doi.org/10.1149/1945-7111/ac6075.

[8] A. Novoselova, V. Smolenski, Electrochemical behavior of neodymium compounds in molten chlorides, Electrochim. Acta. 87 (2013) 657–662. https://doi.org/10.1016/j.electacta.2012.09.064.

[9] D. Shen, R. Akolkar, Electrodeposition of Neodymium from $NdCl_3$-Containing Eutectic

LiCl–KCl Melts Investigated Using Voltammetry and Diffusion-Reaction Modeling, J. Electrochem. Soc. 164 (2017) H5292–H5298. https://doi.org/10.1149/2.0451708jes.

[10] H. Hayashi, M. Akabori, T. Ogawa, K. Minato, Spectrophotometric Study of Nd^{2+} Ions in LiCl-KCl Eutectic Melt, Zeitschrift Für Naturforsch. A. 59 (2004) 705–710. https://doi.org/10.1515/zna-2004-1014.

[11] J. Bruno, R.C. Ewing, Spent nuclear fuel, Elements. 2 (2006) 343–349. https://doi.org/10.2113/gselements.2.6.343.

[12] J.P. Ackerman, T.R. Johnson, Process to remove rare earth from IFR electrolyte, US 5336450; A, 1994.

[13] X. Xi, M. Feng, L. Zhang, Z. Nie, Applications of molten salt and progress of molten salt electrolysis in secondary metal resource recovery, Int. J. Miner. Metall. Mater. 27 (2020) 1599–1617. https://doi.org/10.1007/s12613-020-2175-0.

[14] M. Matsumiya, M. Takano, R. Takagi, R. Fujita, Recovery of Ba Using Liquid Metallic Cathodes in Molten Chlorides, J. Nucl. Sci. Technol. 35 (1998) 836–839. https://doi.org/10.1080/18811248.1998.9733952.

[15] T. Kato, T. Inoue, T. Iwai, Y. Arai, Separation behaviors of actinides from rare-earths in molten salt electrorefining using saturated liquid cadmium cathode, J. Nucl. Mater. 357 (2006) 105–114. https://doi.org/10.1016/j.jnucmat.2006.06.003.

[16] S.Q. Jiao, H.D. Jiao, W.L. Song, M.Y. Wang, J.G. Tu, A review on liquid metals as cathodes for molten salt/oxide electrolysis, Int. J. Miner. Metall. Mater. 27 (2020) 1588–1598. https://doi.org/10.1007/s12613-020-1971-x.

[17] K.M. Goff, A. Schneider, J.E. Battles, Cadmium transport through molten salts in the reprocessing of spent fuel for the integral fast reactor, Nucl. Technol. 102 (1993) 331–340.

https://doi.org/10.13182/NT93-A17032.

[18] D. Yang, S. Jiang, Y. Liu, J. Geng, M. Li, L. Wang, Z. Chai, W. Shi, Electrochemical extraction kinetics of Nd on reactive electrodes, Sep. Purif. Technol. 281 (2022) 119853. https://doi.org/10.1016/j.seppur.2021.119853.

[19] T. Yin, Y. Liu, D. Yang, Y. Yan, G. Wang, Z. Chai, W. Shi, Thermodynamics and Kinetics Properties of Lanthanides (La, Ce, Pr, Nd) on Liquid Bismuth Electrode in LiCl-KCl Molten Salt, J. Electrochem. Soc. 167 (2020) 122507. https://doi.org/10.1149/1945-7111/abb0f4.

[20] T. Lichtenstein, T.P. Nigl, H. Kim, Recovery of Alkaline-Earths into Liquid Bi in Ternary LiCl-KCl-$SrCl_2$/$BaCl_2$ Electrolytes at 500 °C, J. Electrochem. Soc. 167 (2020) 102501. https://doi.org/10.1149/1945-7111/ab9758.

[21] T.P. Nigl, T. Lichtenstein, Y. Kong, H. Kim, Electrochemical Separation of Alkaline-Earth Elements from Molten Salts Using Liquid Metal Electrodes, ACS Sustain. Chem. Eng. 8 (2020) 14818–14824. https://doi.org/10.1021/acssuschemeng.0c04249.

[22] S. Im, S.L. Shang, N.D. Smith, A.M. Krajewski, T. Lichtenstein, H. Sun, B.J. Bocklund, Z.K. Liu, H. Kim, Thermodynamic properties of the Nd-Bi system via emf measurements, DFT calculations, machine learning, and CALPHAD modeling, Acta Mater. 223 (2022) 117448. https://doi.org/10.1016/j.actamat.2021.117448.

[23] N.G. Kulagina, A.P. Bayanov, An Electromotive Force Study of the Thermodynamic Properties of Neodymium Tristannide and Its Solutions in Liquid Tin, Russ. J. Phys. Chem. 48 (1974) 466–467.

[24] T. Lichtenstein, S. Im, C.T. Yu, H. Kim, Thermodynamic properties of rare-earth alloys by electrochemical emf measurements, J. Mater. Res. (2021) 1–9. https://doi.org/10.1557/jmr.2020.218.

[25] S. Im, N.D. Smith, S.C. Baldivieso, H. Kim, Electrochemical Cell Design for Emf Measurements of Liquid Nd-Bi Alloys via Coulombic Titration in LiCl-KCl-$NdCl_3$ Electrolyte, in: T. Ouchi, G. Azimi, K. Forsberg, H. Kim, S. Alam, N.R. Neelameggham, A.A. Baba, H. Peng (Eds.), Rare Met. Technol. 2022, Springer International Publishing, Cham, 2022: pp. 317–324.

[26] Z. Lu, J. Jiang, M. Ren, J. Xu, J. Da, F. Cao, The study on removing the salts in crude oil via ethylene glycol extraction, Energy and Fuels. 29 (2015) 355–360. https://doi.org/10.1021/ef502453j.

[27] V.N. Eremenko, M. V. Bulanova, P.S. Martsenyuk, Phase diagram of the Neodymium-Tin system, Sov. Prog. Chem. 54 (1988) 8–11.

[28] K. Yoshihara, J.B. Taylor, L.D. Calvert, J.G. Despault, Rare-earth bismuthides, J. Less-Common Met. 41 (1975) 329–337. https://doi.org/10.1016/0022-5088(75)90038-7.

[29] L. Wang, Q. Wang, A. Xian, K. Lu, Precise measurement of the densities of liquid Bi, Sn, Pb and Sb, J. Phys. Condens. Matter. 15 (2003) 777. https://doi.org/10.1088/0953-8984/15/6/304.

[30] F. Weitzer, K. Hiebl, P. Rogl, Crystal chemistry and magnetism of neodymium stannides including compounds of the structural series RE_nSn_{3n-2}, J. Solid State Chem. 98 (1992) 291–300. https://doi.org/10.1016/S0022-4596(05)80237-3.

[31] A. Kuriyama, K. Hosokawa, H. Konishi, H. Ono, E. Takeuchi, T. Nohira, T. Oishi, Electrochemical Formation of RE-Sn (RE=Dy, Nd) Alloys Using Liquid Sn Electrodes in a Molten LiCl-KCl System, ECS Trans. 75 (2016) 341–348. https://doi.org/10.1149/07515.0341ecst.

[32] A.J. Bard, L.R. Faulkner, Electrochemical Methods: Fundamentals and Applications, Wiley,

2001.

FIGURES

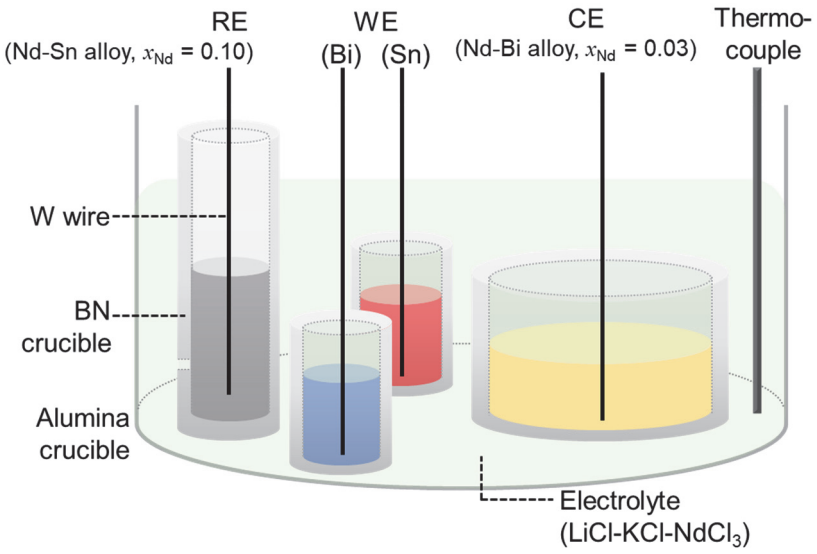

Fig. 1. Three-electrode electrochemical cell for emf measurement of the Nd-Sn alloys via coulometric titration and Nd recovery into liquid metals (Bi and Sn).

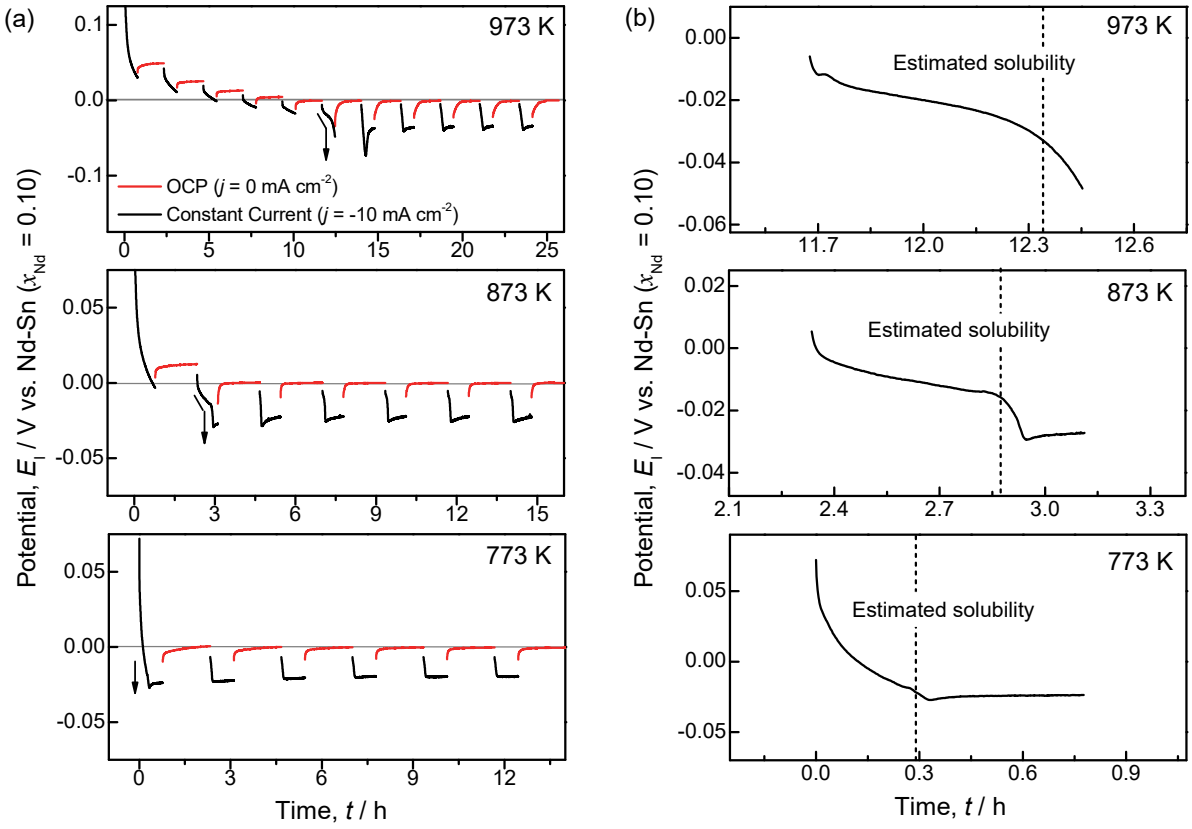

Fig. 2. (a) Coulometric titration of Nd into liquid Sn using constant current (–10 mA cm^{-2}) followed by OCP measurements at T = 773−973 K, and (b) titration step with steep potential drop indicated by downward arrow (↓) in (a).

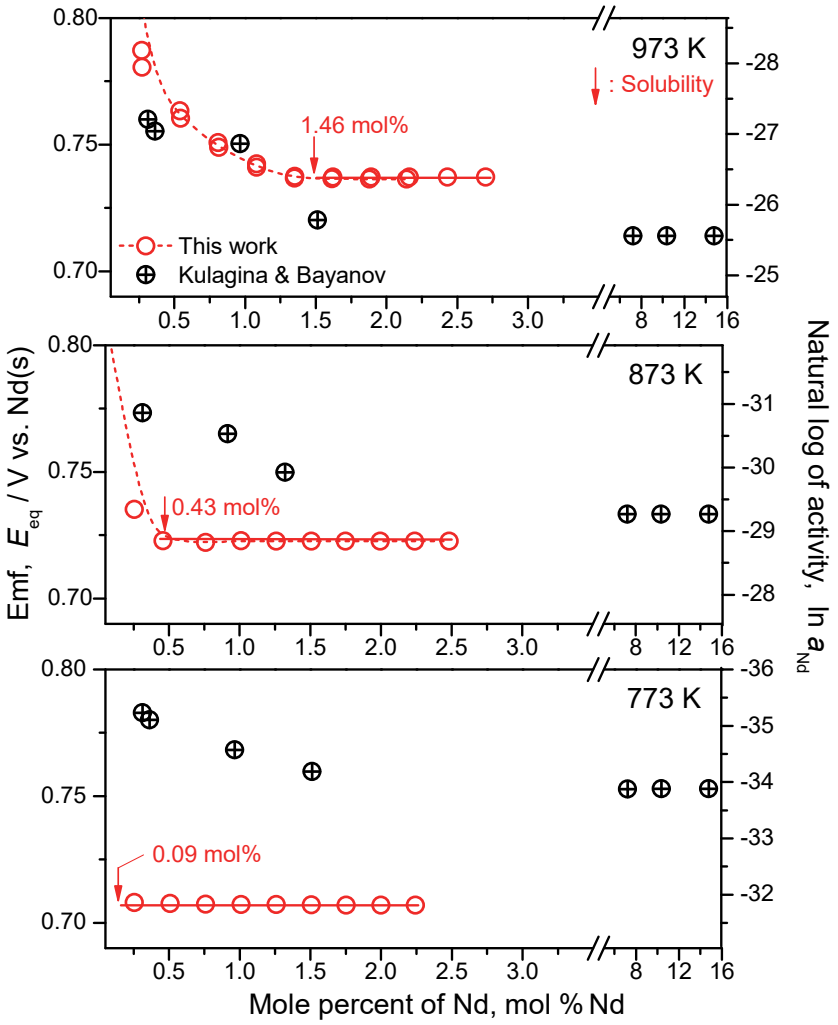

Fig. 3. Emf and activity of Nd-Sn alloys as a function of Nd mole percent at 773–973 K in comparison to the results by Kulagina and Bayanov [23].

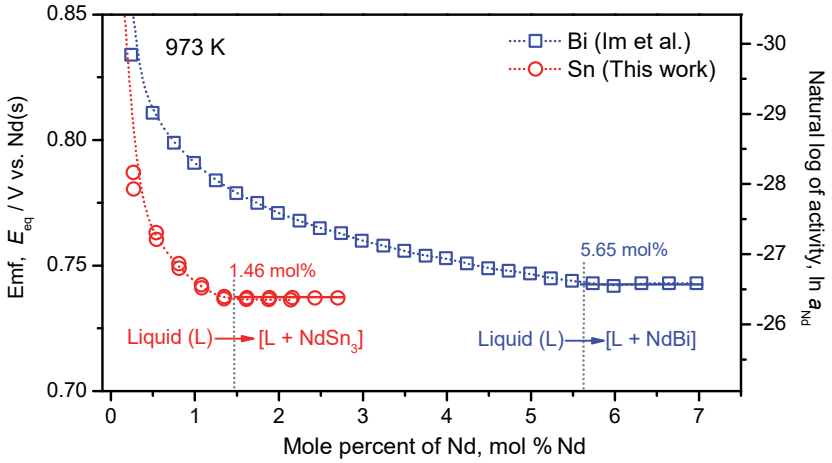

Fig. 4. Comparison of emf and activity of Nd-Bi and Nd-Sn alloys as a function of Nd mole percent at 973K, where Nd solubility is estimated from the intersection of distinct emf trajectories [22].

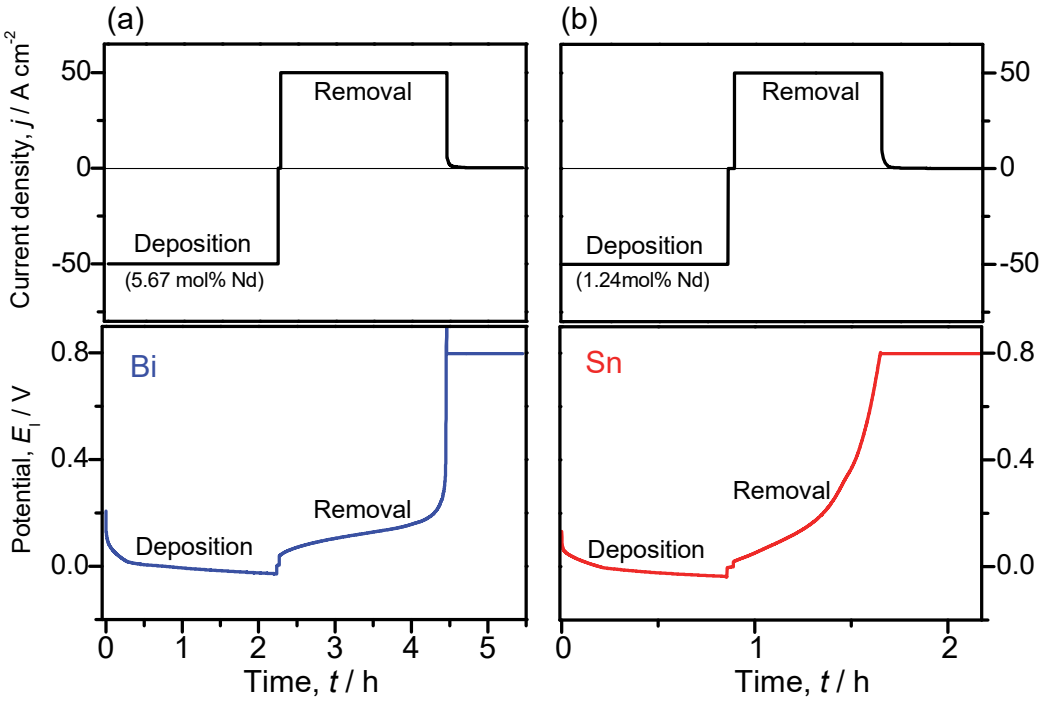

Fig. 5. Representative deposition-removal cycle of (a) Bi and (b) Sn electrodes using constant current (±50 mA cm^{-2}) at 973 K for an estimation of the round-trip coulombic efficiency ($q_{deposition}/q_{removal}$) where q is the charge applied during each step.

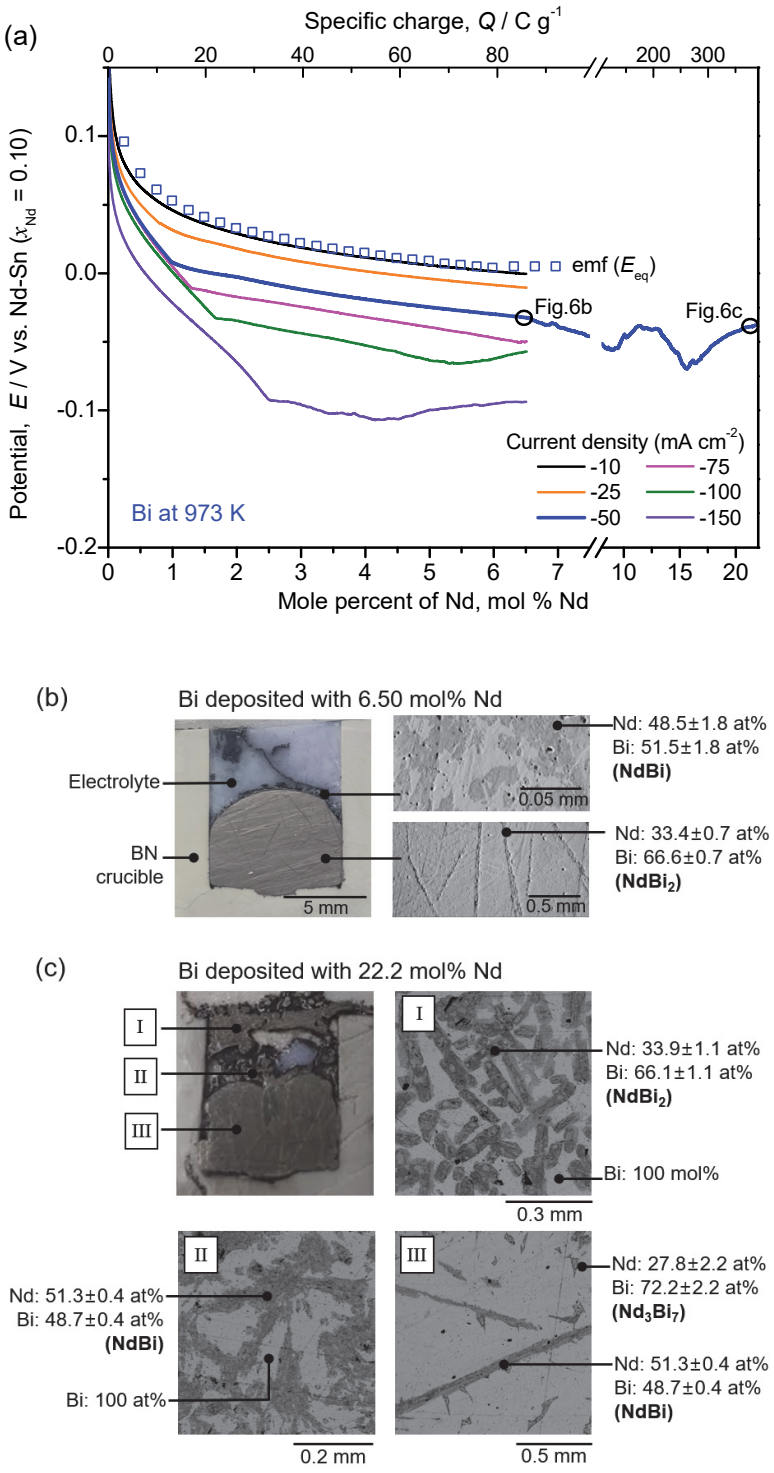

Fig. 6. (a) Electrode potential of liquid Bi during Nd deposition using constant currents at 10−150 mA cm^{-2} at 973 K, and (b-c) cross-section images of Bi electrodes after constant current electrolysis (50 mA cm^{-2}) using optical and electron microscopes, deposited at (b) 6.50 mol% Nd and (c) 22.2 mol% Nd. Suggested intermetallic compound in the parenthesis based on EDS analysis.

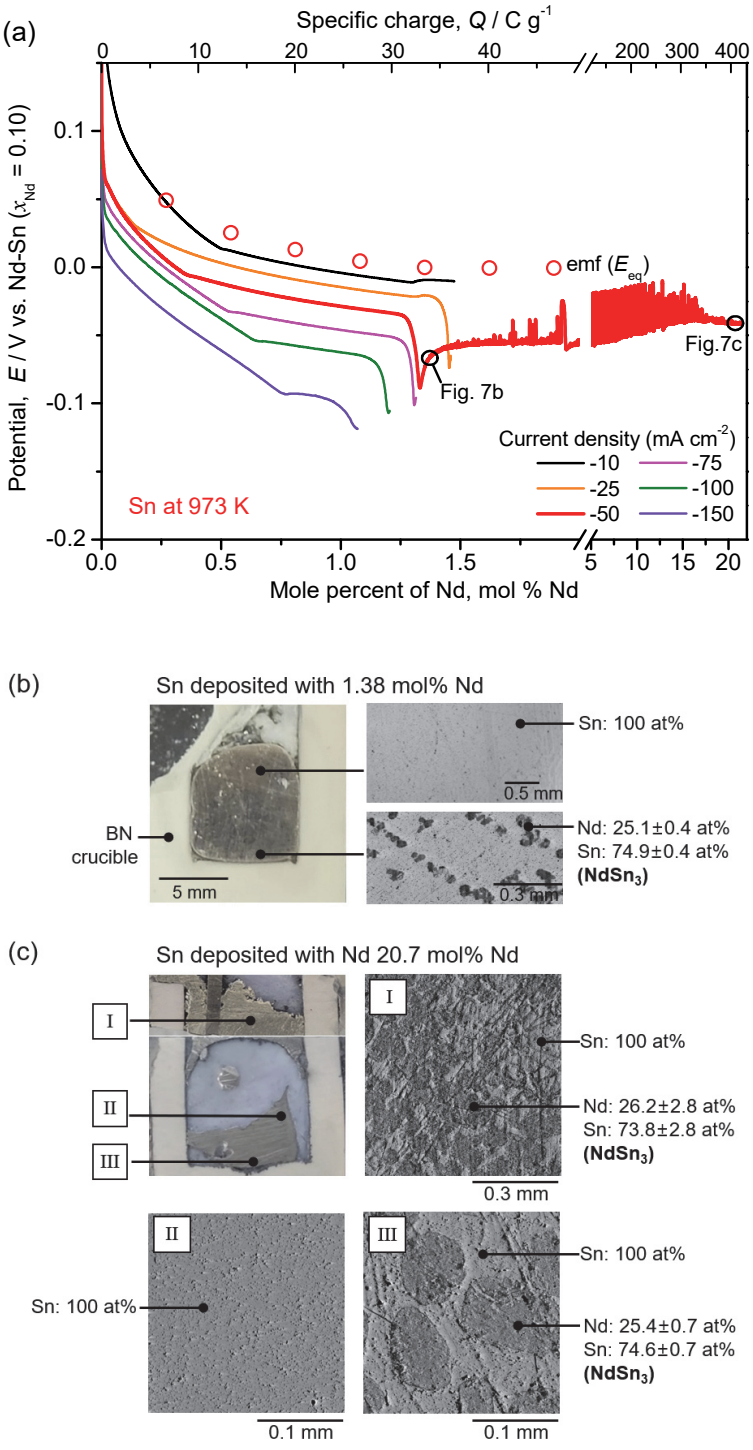

Fig. 7. (a) Electrode potential of liquid Sn during Nd deposition using constant currents at 10−150 mA cm^{-2} at 973 K, and (b-c) cross-section images of Sn electrodes after constant current electrolysis (50 mA cm^{-2}) using optical and electron microscopes, deposited at (b) 1.38 mol% Nd and (c) 20.7 mol% Nd. Suggested intermetallic compounds in the parenthesis based on EDS analysis.

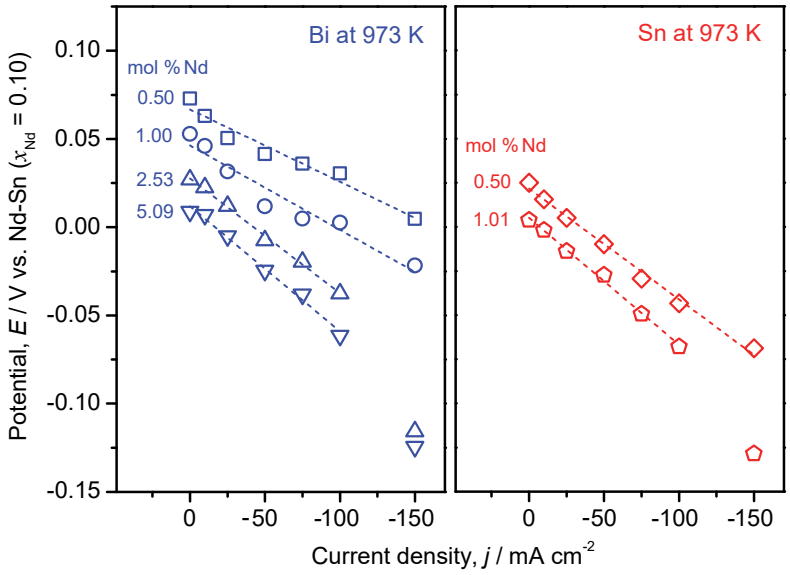

Fig. 8. Potential of Bi and Sn electrodes as a function of the current density (j = -10−150 mA cm^{-2}) for selected mol% Nd at 973 K. Dashed lines are linear fits.

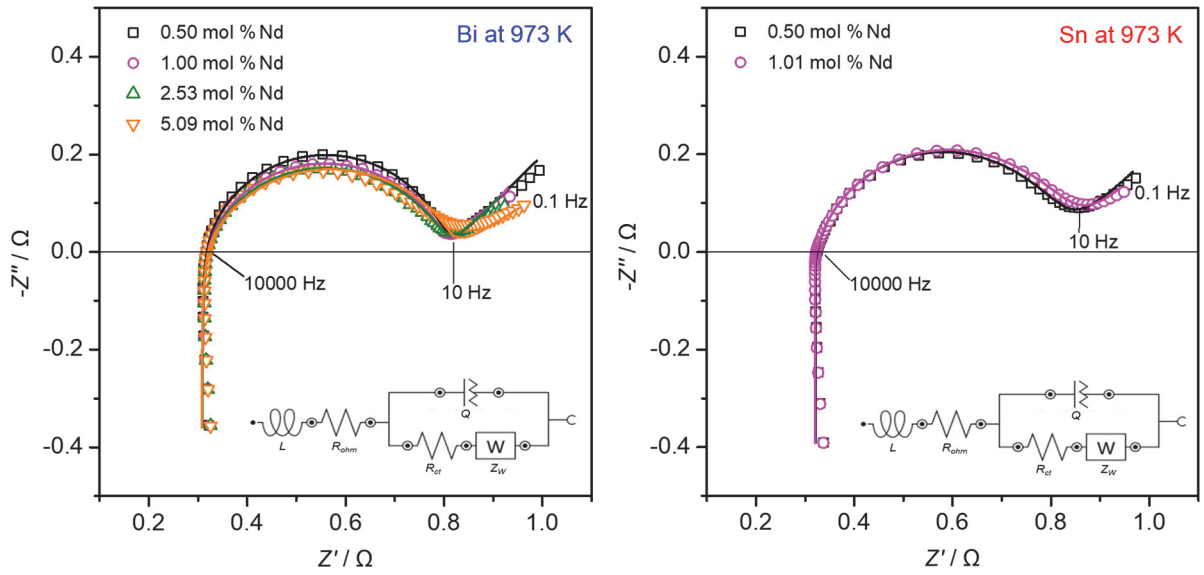

Fig. 9. Nyquist plot of liquid Bi (left) and Sn (right) electrodes with selected Nd concentration at 973 K, fitted (solid lines) using an equivalent circuit model (in the inset).

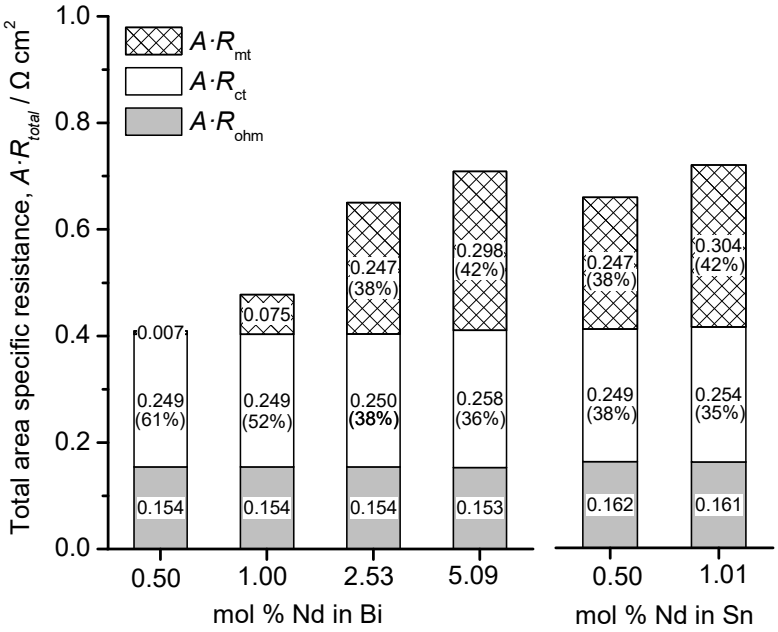

Fig. 10. Relative contribution of each area-specific resistance in the total resistance of the liquid Bi and Sn electrodes at selected compositions during electrolysis at 973 K.

TABLES

Table 1. Measured emf (E_{eq}), natural logarithm of activity ($\mathbf{ln}\boldsymbol{a}_{\mathbf{Nd}}$), and excess partial molar Gibbs energy ($\Delta\bar{\boldsymbol{G}}_{\boldsymbol{Nd}}^{\boldsymbol{E}}$) of Nd in liquid Sn at T = 773−973 K.

mol%$_{Nd}$	E_{eq}(V)			lna_{Nd}			$\Delta\bar{G}_{Nd}^{E}$ (kJ mol^{-1})		
	773 K	873 K	973 K	773 K	873 K	973 K	773 K	873 K	973 K
0.255	0.708	0.735	0.787	-31.89	-29.32	-28.17	-166.6	-169.5	-179.5
0.508	0.708	0.723	0.763	-31.87	-28.83	-27.31	-170.9	-170.9	-178.2
0.760	0.707	0.723	0.751	-31.86	-28.83	-26.87	-173.4	-173.8	-177.9
1.011	0.707	0.723	0.742	-31.85	-28.82	-26.56	-175.2	-175.9	-177.7
1.260	0.707	0.723	0.737	-31.85	-28.82	-26.39	-176.6	-177.4	-178.1
1.508	0.707	0.723	0.737	-31.85	-28.82	-26.38	-177.7	-178.7	-179.5
1.755	0.707	0.723	0.737	-31.84	-28.82	-26.38	-178.7	-179.8	-180.7
2.000	0.707	0.723	0.737	-31.84	-28.82	-26.38	-179.5	-180.8	-181.7
2.245	0.707	0.723	0.737	-31.84	-28.82	-26.38	-180.2	-181.6	-182.7
2.488	–	0.723	0.737	–	-28.82	-26.38	–	-182.4	-183.5

Table 2. The solubility of Nd (mol %) in liquid Sn and Bi at T = 773−973 K.

Temperature	liquid Sn			liquid Bi
	This work	Eremenko [27]	Kulagina [23]	Im [22]
773 K	0.09	1.50	1.90	0.99
873 K	0.43	3.00	2.09	2.91
973 K	1.46	4.50	3.02	5.65

Table 3. Chemical composition of electrolysis products for Bi electrode by ICP-AES, the charge ($q_{measured}$) equivalent to the measured Nd contents, and the Faradaic efficiencies relative to the applied charge ($q_{applied}$).

T	$q_{applied}$ (mol% Nd)	Composition of electrolysis products by ICP and IC (wt%)					Corrected results (wt%)*		$q_{measured}$ (mol% Nd)	Faradaic efficiency
		Bi	Li	K	Nd	Cl	Bi	Nd		
973 K	96 C g^{-1} (6.50)	94.65	0.02	0.15	4.72	0.46	95.58	4.42	87 C g^{-1} (5.87)	89.8 %
	394 C g^{-1} (22.2)	84.83	0.03	0.19	14.65	0.30	85.27	14.73	347 C g^{-1} (20.0)	87.9 %
	405 C g^{-1} (21.9)	85.12	0.00	0.04	14.66	0.17	85.49	14.51	340 C g^{-1} (19.7)	84.1 %
873 K	389 C g^{-1} (21.8)	84.52	0.00	0.04	14.90	0.53	85.66	14.34	335 C g^{-1} (19.5)	86.0 %

*Results were corrected by subtracting the residual salt content in the electrode sample based on Cl concentration measured via ion chromatography by assuming Li as LiCl, K as KCl, and the remaining Cl as $NdCl_3$.

Table 4. Estimated total area-specific resistances ($A{\cdot}R_{total}$) at 973 K from *I-V* curve (**Fig. 8**) and impedance spectra (**Fig. 9**) based on the equivalent circuit model *LR(Q(RW))*.

	mol% Nd	$A{\cdot}R_{total}$ (Ω cm^2)	$A{\cdot}R_{ohmic}$ (Ω cm^2)	$A{\cdot}R_{ct}$ (Ω cm^2)	Q (mS)	n*	W (S)	L (fH)	χ^2	j_0 (A cm^{-2})
Bi	0.50	0.410	0.154	0.249	0.002	0.87	4.79	0.57	0.004	0.225
	1.00	0.478	0.154	0.249	0.004	0.81	6.90	0.58	0.004	0.225
	2.53	0.651	0.154	0.250	0.006	0.77	7.97	0.58	0.009	0.224
	5.09	0.709	0.153	0.258	0.009	0.74	6.66	0.58	0.023	0.217
Sn	0.50	0.658	0.162	0.249	0.029	0.87	5.67	0.62	0.007	0.225
	1.01	0.719	0.161	0.254	0.058	0.86	7.45	0.58	0.007	0.220

* Impedance (Z_Q) of the constant phase element: $1/Z_Q = Q(j\omega)^n$